
Figures and figure supplements

Proliferative exhausted CD8⁺ T cells exacerbate long-lasting anti-tumor effects in human papillomavirus-positive head and neck squamous cell carcinoma

Danni Cheng, Ke Qiu and Yufang Rao *et al.*

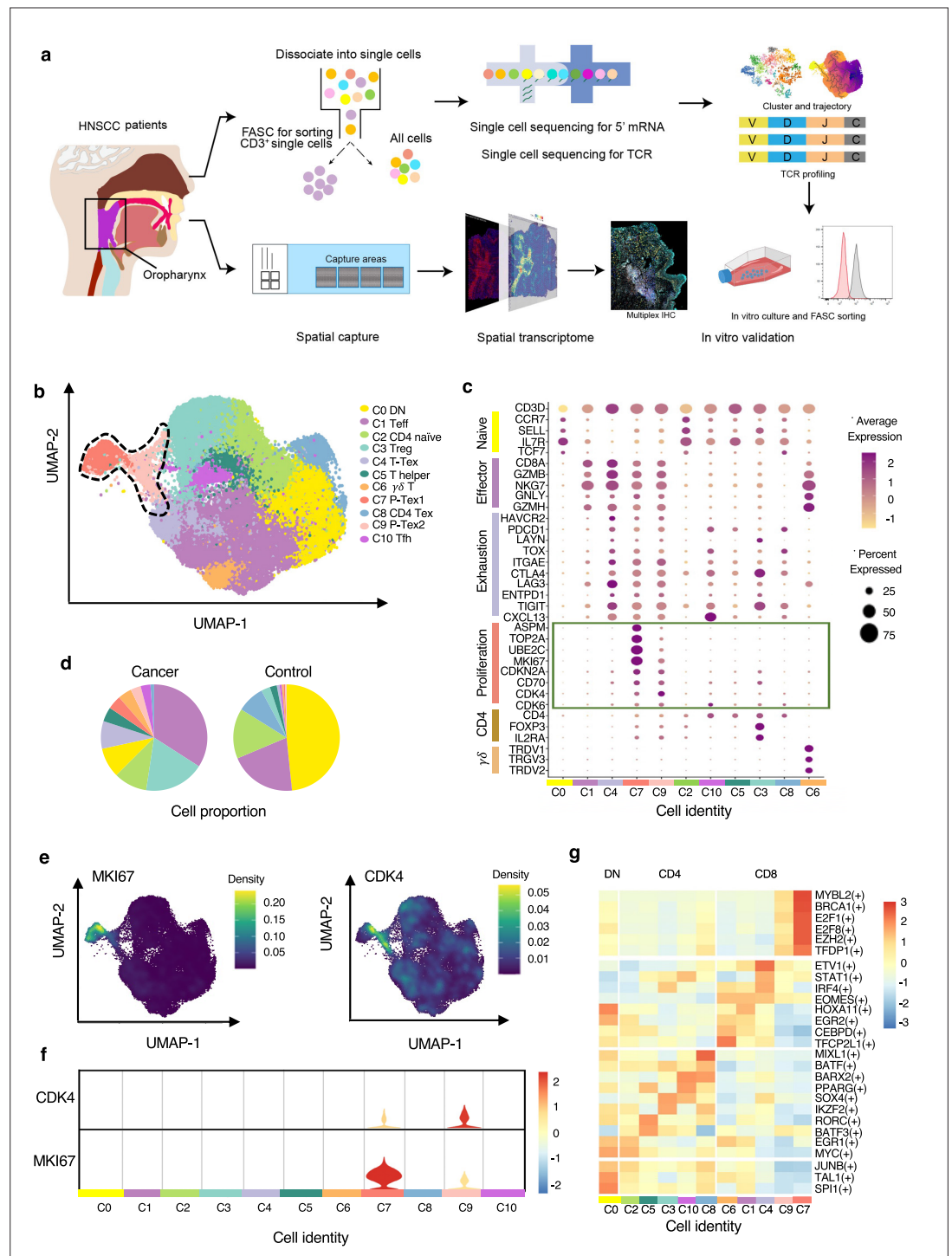


Figure 1. The P-Tex cell clusters identified in the T cell landscapes of head and neck squamous cell carcinoma (HNSCC) patients by single-cell RNA sequencing (scRNA-seq). **(a)** The flow chart of this study. **(b)** Uniform manifold approximation and projection (UMAP) plot of all single T cells from 14 samples via 10× Genomics. Eleven T cell clusters with different functions are identified. **(c)** Dotplot of selected T cell function-associated genes across different T cell clusters, showing both gene expression level (the color gradient) and the percentage of cells (the size of circle) in a given cluster. **(d)** Pie charts of cell-type fractions identified in cancer and normal adjacent tissues, colored by cell types. **(e)** The kernel density estimation plot showing the distribution of MKI67 and CDK4 genes of T cells. **(f)** The gene expression levels of CDK4 and MKI67 shown by violin plots. **(g)** Heatmap of the transcriptional regulators of top expressed genes in each T cell clusters.

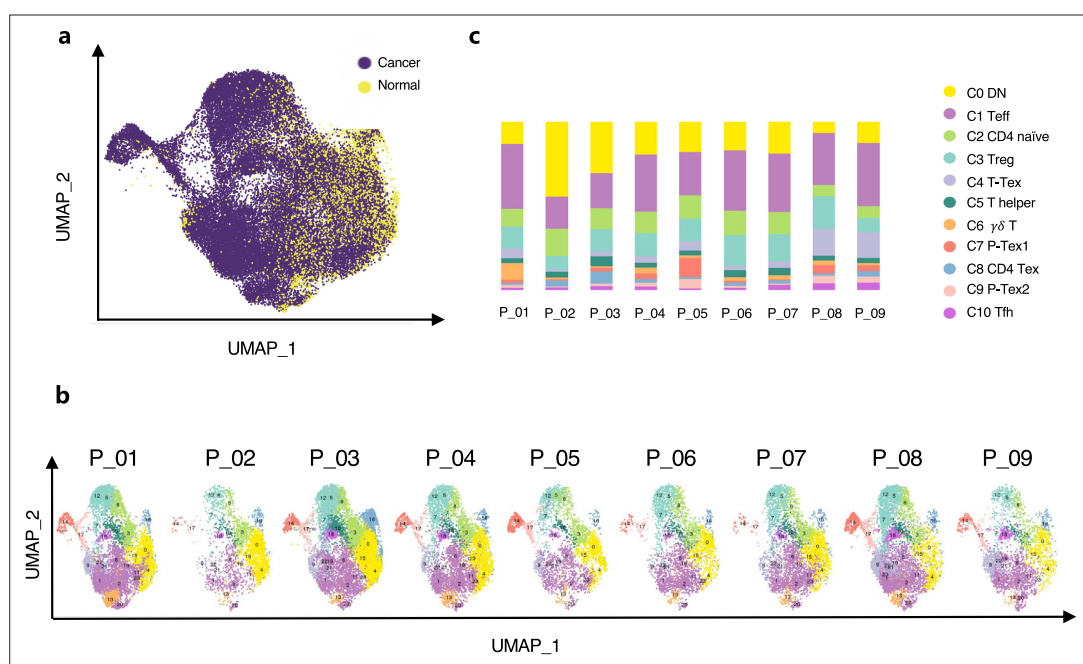


Figure 1—figure supplement 1. The extended summary of functional properties of T cell clusters in **Figure 1**. (a) The distribution of T cells in cancer and adjacent normal tissues in uniform manifold approximation and projection (UMAP) plots. (b) The distribution of T cells in each patient in UMAP plots. (c) The distribution of cell proportions in each sample.

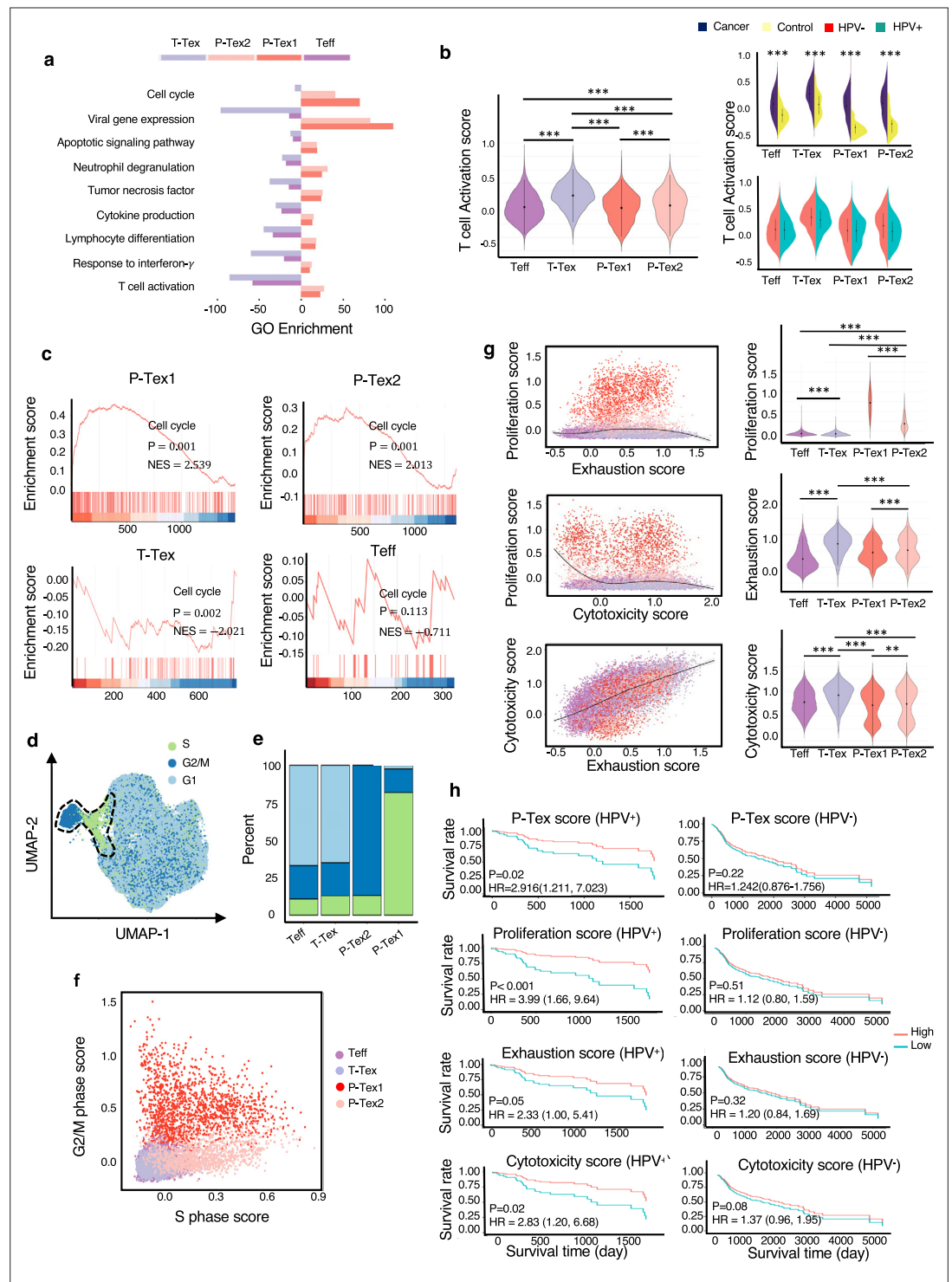


Figure 2. The comparison of functional characteristics between P-Texs and other CD8⁺ T cell clusters. (a) Gene ontology (GO) analysis of differentially expressed genes in each CD8⁺ T cell clusters, colored by cell types. (b) The T cell activation score of each CD8⁺ T cell clusters. T cell activation score defined as the averaged expression of genes in the activation signature in **Supplementary file 3**. Statistics were assessed by Dunn's tests. (c) The gene set enrichment analysis (GSEA) diagrams show the enrichment profiles of cell cycle pathway in each CD8⁺ T cell clusters. (d-f) The distribution and scores of cell cycle phases of each CD8⁺ T cells. (g) The proliferation, exhaustion, and cytotoxic scores of each CD8⁺ T cell clusters. Proliferation score: averaged expression of MKI67-related genes; exhaustion score: averaged expression of PDCD1-related genes; cytotoxic score: averaged

Figure 2 continued on next page

Figure 2 continued

expression of GZMB-related genes. **(h)** The Kaplan–Meier curves show the overall survival rate of HPV⁺/HPV[−] head and neck squamous cell carcinoma (HNSCC) patients with different proliferation, exhaustion, and cytotoxic scores in The Cancer Genome Atlas (TCGA) cohort, adjusted for age and gender. ***: $p < 0.001$, **: $p < 0.01$, *: $p < 0.05$.

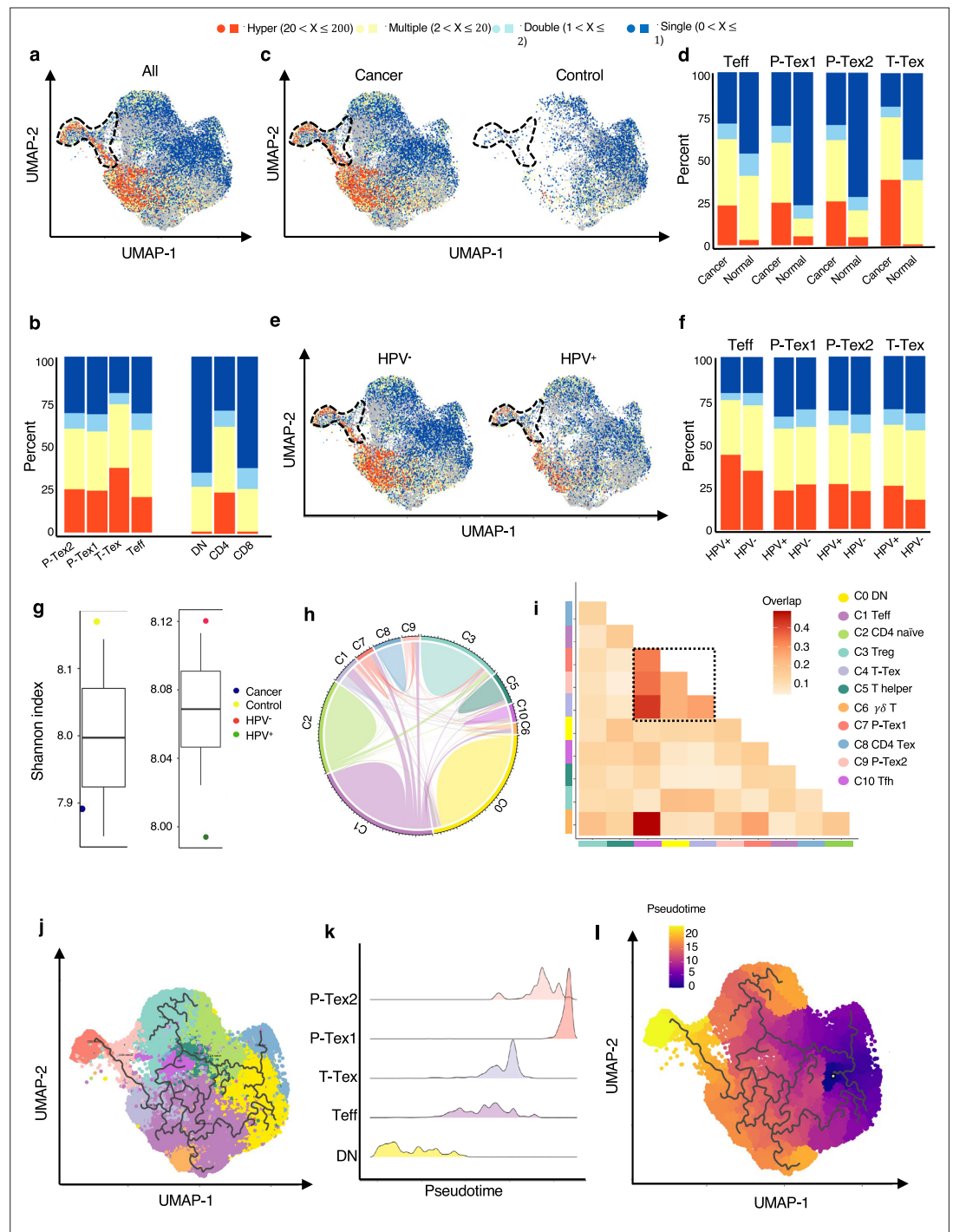


Figure 3. The developmental trajectory and lineage relationships among T cell clusters. (a–f) Single-cell TCR profiling of head and neck squamous cell carcinoma (HNSCC) in all samples (a–b), cancer tissues vs. normal tissues (c–d), HPV+ vs. HPV- (e–f). Bar plots show the fractions of each clonotype frequencies. The clonotype frequencies are defined as unique ($n=1$), double ($n=2$), multiple clones ($2 < n \leq 20$), and hyper clones ($20 < n \leq 200$) according to the numbers of clonotypes. (g) The TCR diversity of cancer tissues vs. normal tissues and HPV+ vs. HPV- samples, calculated using Shannon metric. (h–i) Cell state transition of T cell clusters inferred by shared TCRs. The chord diagram (h) showing the fraction of shared clonotypes among each cell clusters. Lines connecting different clusters are based on the degree of TCR sharing, with the width of lines representing the number of shared TCRs. The clonal overlap diagram (i) measures the clonal similarity among each cluster. Color gradient in the grid refers to the overlap coefficient. The higher the index score, the higher the clonal diversity. (j–l) Potential developmental trajectory of T cells inferred by Monocle3 based on gene expressions.

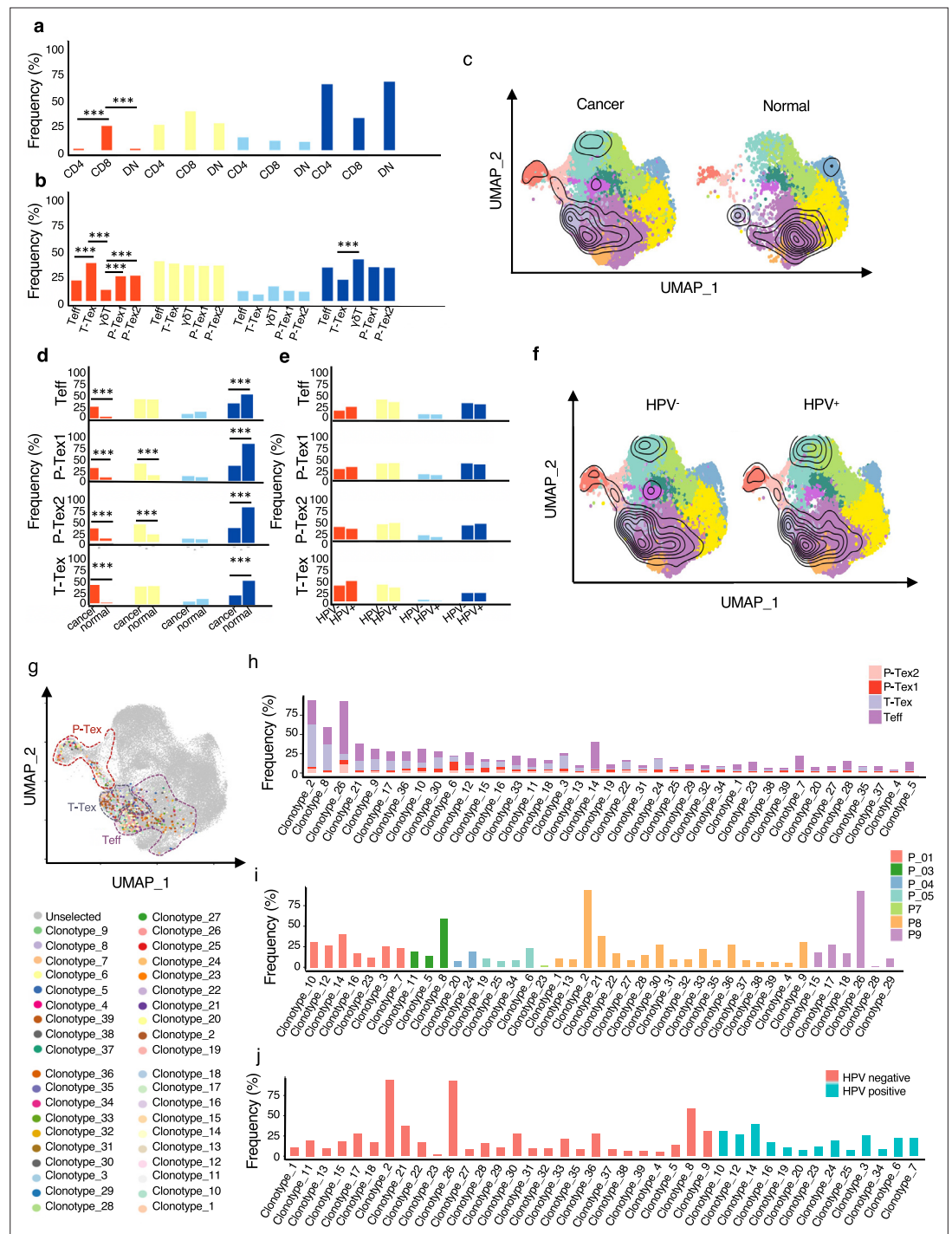


Figure 3—figure supplement 1. Extended summary of TCR properties of **Figure 3**. The supplementary comparison of the clonotype frequencies of clusters in each cluster (**a–b**), cancer tissues vs. normal tissues (**c–d**), HPV+ vs. HPV- (**e–f**); statistics were assessed by Chi-square tests. The clonotypes are defined as unique (n=1), double (n=2), multiple (2 < n ≤ 20), and hyper clonal (20 < n ≤ 200) according to their clonotype numbers. The clonalOverlay diagrams show the clonal expansion in HPV+ vs. HPV- and cancer tissues vs. normal tissues by overlaying the cells with specific clonal frequency onto the uniform manifold approximation and projection (UMAP) plots in Seurat (**c and f**). The density contours indicate the frequencies of TCR, with the number of clones ≥3 to be the cutoff value of the outermost circle layer, and the most central circle layer represents the area with the highest TCR expansion. (**g–j**) The distribution of shared CD8+ clones on the UMAP plot. Colored dots were CD8+ T cells of identical clonotypes. The colored circles highlight the cluster information of each cell, as defined in **Figure 1a**, with **Figure 3—figure supplement 1 continued on next page**

Figure 3—figure supplement 1 continued

fractional Teff, T-TEX, and P-TEX cells sharing the same TCRs shown in colors. Bar charts show the proportion of the each clonotype in each cluster (**h**), samples (**i**), and different human papillomavirus (HPV) status (**j**), respectively. ***: $p < 0.001$, **: $p < 0.01$, *: $p < 0.05$.

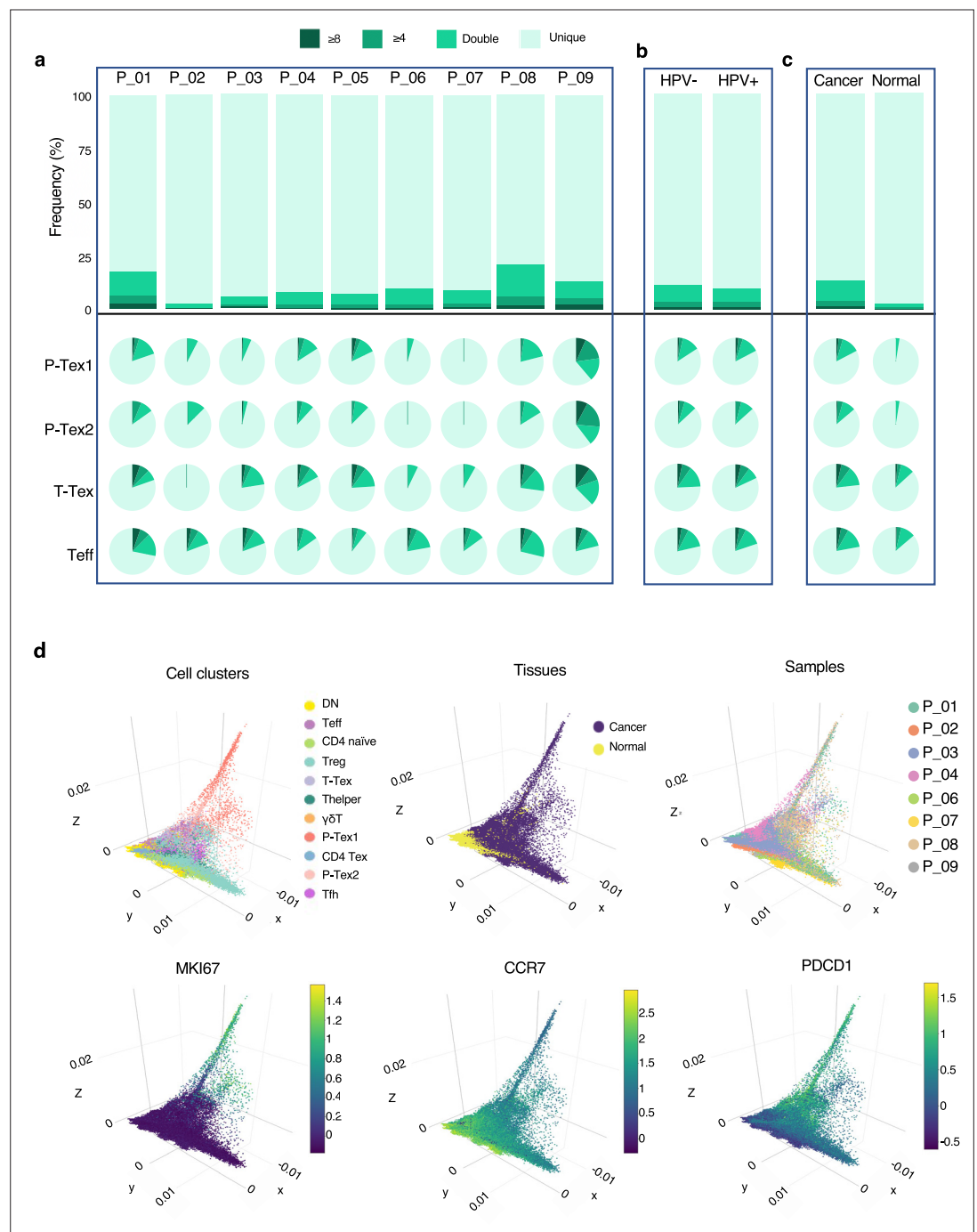


Figure 3—figure supplement 2. Extended summary of TCR clonotypes and potential differentiation direction of **Figure 3**. (a–c) The frequency of clonotypes and TCR distribution of CD8⁺ T cells across individuals (a), HPV⁺/HPV[−] samples (b), and cancer/normal samples (c). Frequencies of TCRs are labeled with gradient colors. Pie charts below each bar illustrate the TCR composition of each CD8 cluster. (d) The 3D developmental trajectories of T cells show the potential differentiation direction of each cluster.

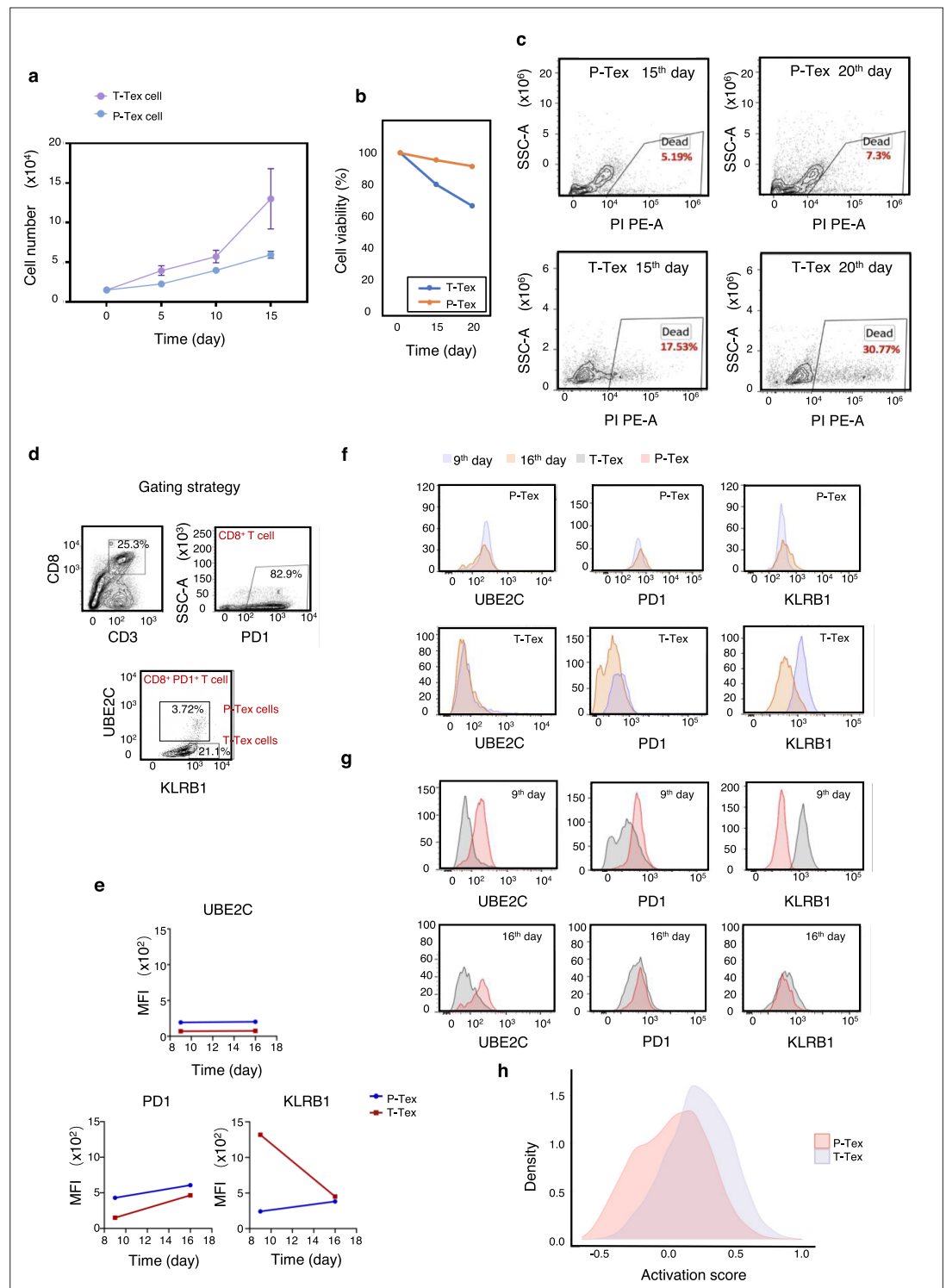


Figure 4. The survival and proliferation capacity of P-Texs in vitro. Comparing the proliferation (a) and survival (b–c) capacity of P-Tex and T-Tex cells cultured with IL-2 for 15 and 20 days in vitro measured by CCK8 experiment; proliferation experiment, shown by the mean ± SEM. (d–g) Representative flow cytometry assay of UBE2C, PD1, and KLRB1 of P-Tex cells after 9 and 15 days of stimulation with anti-CD3/CD28 microbeads in vitro. (d) The gating strategies of PD1, KLRB1, and UBE2C. (e–g) Mean fluorescence intensity (e) and cell count (f–g) of UBE2C, PD1, and KLRB1 in P-Tex and T-Tex cells at different days detected by flow cytometry. (h) Histogram of activation states of P-Tex and T-Tex cells by single-cell RNA-seq data.

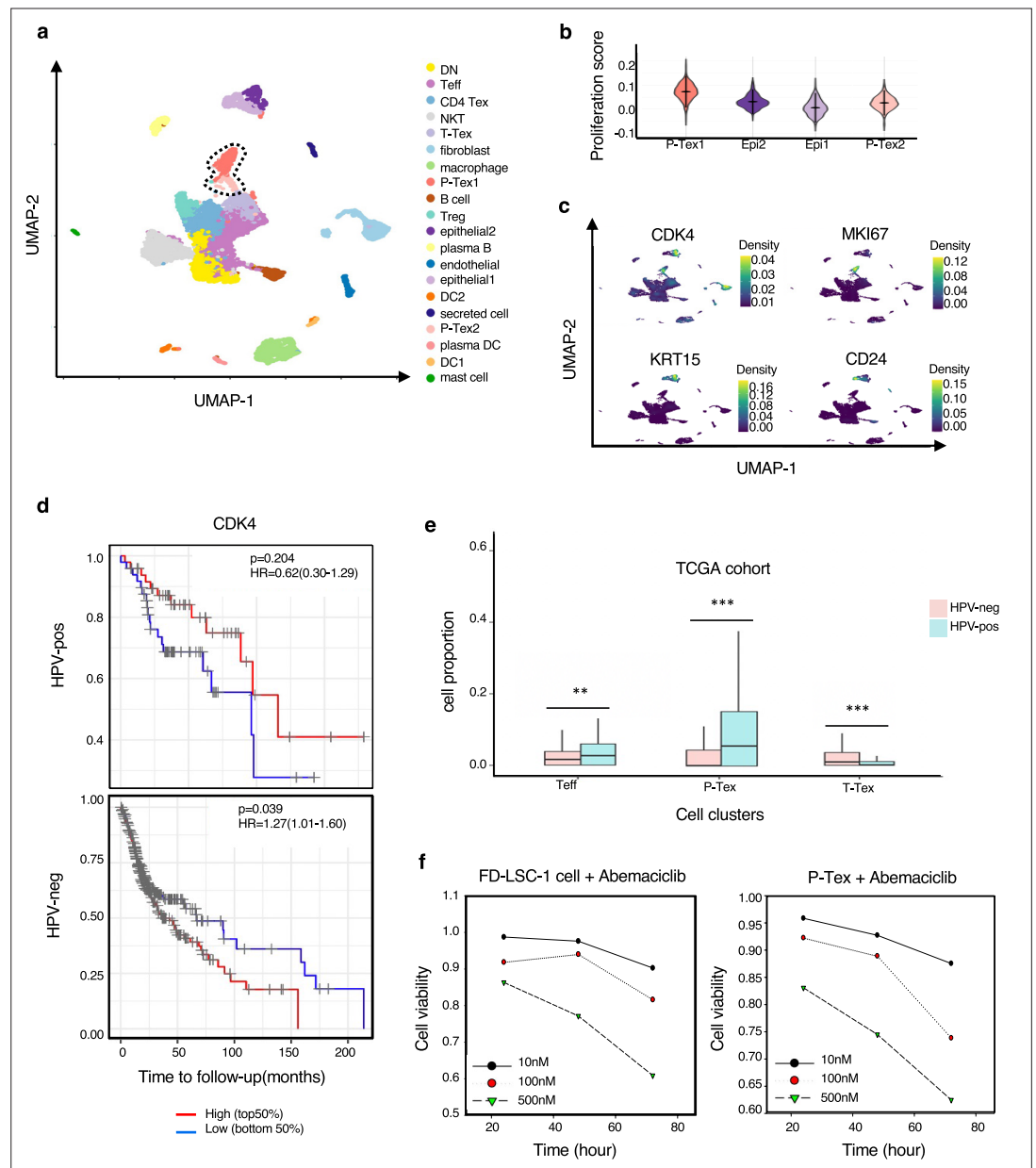


Figure 5. The expression of CDK4 gene in P-Tex2 cluster is associated with the treatment outcomes of HPV⁺ head and neck squamous cell carcinoma (HNSCC) patients. **(a)** Single-cell transcriptomic profiling of HNSCC tumor microenvironment (TME). Twenty cell clusters are identified, colored by cell types. **(b)** The proliferation status of P-Tex and epithelial cells in violin plot. **(c)** The kernel density estimate distribution of proliferation markers (CDK4 and MKI67) and epithelial cancer cell markers (KRT15 and CD24) in uniform manifold approximation and projection (UMAP) plots. **(d)** The overall survival rate of HPV⁺/HPV⁻ HNSCC patients in The Cancer Genome Atlas (TCGA) cohort related to the expression levels of CDK4 gene, adjusted for age and gender. **(e)** The proportion of P-Texs, T-Tex, and TEFF clusters in HPV⁺ and HPV⁻ samples in TCGA cohort by using the deconvolution algorithm; statistics were assessed by Chi-square tests. Marker genes that were used to define cell clusters in **(a)** are deconvolved into the TCGA data to obtain the proportion of P-Texs, T-Tex, and Teff clusters in the TCGA cohort. **(f)** The cell viability of P-Tex and cancer epithelial cells assessed by CCK8 experiment after Abemaciclib treated in vitro. ***: $p < 0.001$, **: $p < 0.01$, *: $p < 0.05$.

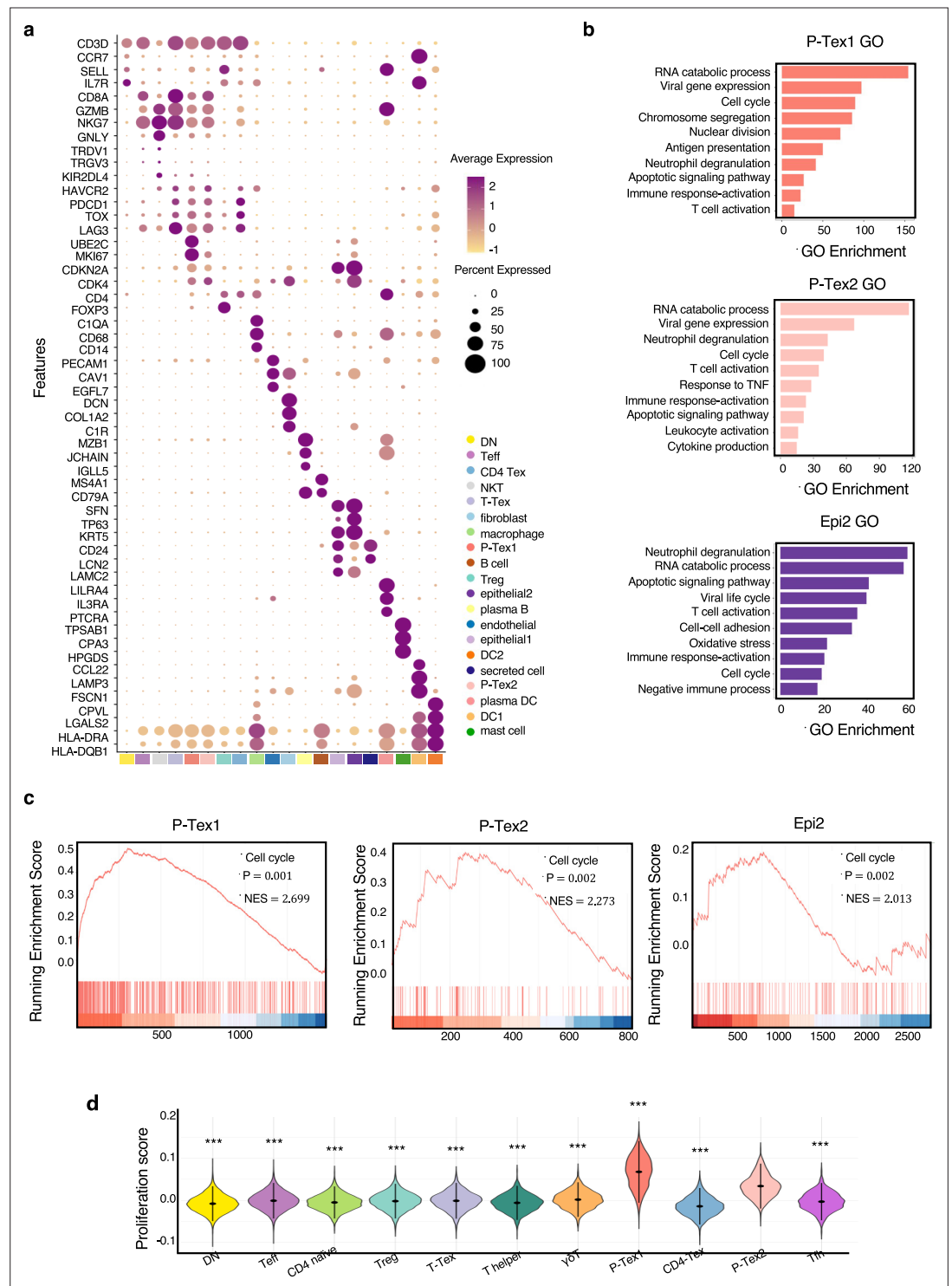


Figure 5—figure supplement 1. The extended summary of functional properties of cell clusters in **Figure 5**. **(a)** Average expression of selected T cell function-associated genes across different cell clusters. **(b)** Gene ontology (GO) analysis of differentially expressed genes in two P-Tex and cancer epithelial cell clusters. **(c)** The gene set enrichment analysis (GSEA) diagrams show the enrichment of cell cycle genes in P-Tex clusters and cancer epithelia cluster. **(d)** The proliferation status of each T cell cluster; statistics were assessed by Dunn's tests. ***: $p < 0.001$, **: $p < 0.01$, *: $p < 0.05$.

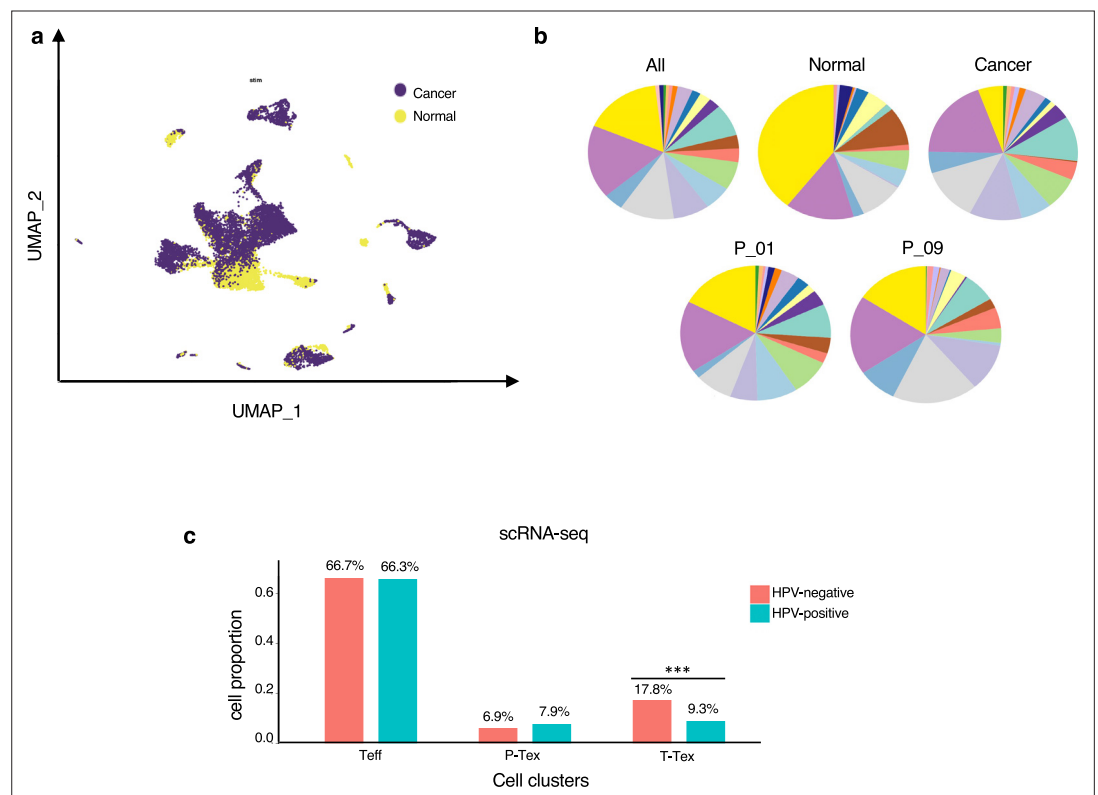


Figure 5—figure supplement 2. The extended summary of function properties of cell clusters in **Figure 5**. **(a)** The distribution of cells in cancer and normal tissues in uniform manifold approximation and projection (UMAP) plots. **(b)** The proportion of each cell cluster in all samples, cancer vs. normal tissue samples, and individual samples, colored by cell types. **(c)** Comparing the proportion of P-Texs, T-Tex, and Teff clusters in HPV⁺ and HPV⁻ samples in single-cell sequencing data; statistics were assessed by Chi-square tests. ***: $p < 0.001$, **: $p < 0.01$, *: $p < 0.05$.

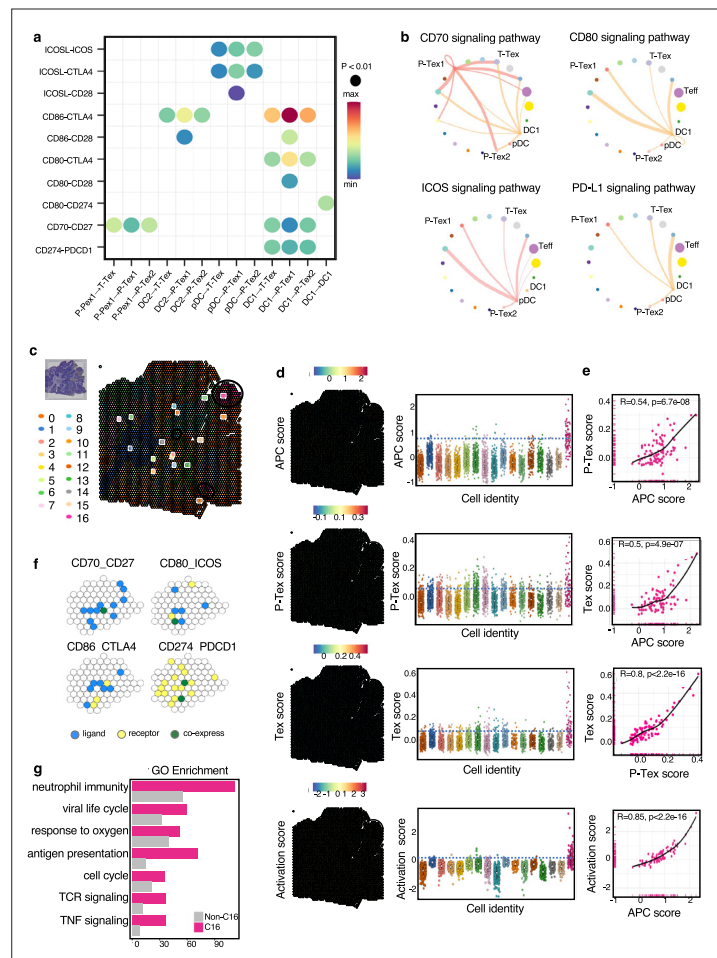


Figure 6. The cell-cell interactions between T cells and APC cells are enriched in the proliferation and cell activation pathways in head and neck squamous cell carcinoma (HNSCC) tumor microenvironment (TME). **(a)** The communication probabilities mediated by selected ligand–receptor pairs among different cell types. The color gradient shows the level of interaction. **(b)** Network circle graphs visualize the inferred communication network of signaling pathways among different cell clusters derived by ligand–receptor interactions. The color of lines are consistent with the ligands. The width of lines are proportional to the interaction strength, and the circle sizes are proportional to the number of cells in each clusters. **(c)** The spatial transcriptomic landscape of representative HNSCC samples. **(d–e)** P-Tex and Tex features were co-expressed in APC area (cluster 16). The circles in SpatialDimPlot **(d, left)** represent APC, P-Tex, and Tex scores enriched in the APC area (cluster 16). The Texs and P-Tex scores were higher in the APC aggregation area **(d, right)**. The correlation of P-Tex, Tex, activation scores, and APC scores in the spatial transcriptome **(e)**. **(f)** Spatial feature plots of selected ligands–receptor interactions enriched in APC area. Spatial feature plots showing the expression pattern of single ligand genes (CD70, CD80, CD86, CD274, yellow spots), single receptor genes (CD27, ICOS, CTLA4, PDCD1, blue spots), and co-expression pattern (green spots) in APC area. **(g)** Gene ontology (GO) analysis identified the enriched gene functions in APC area of spatial transcriptome.

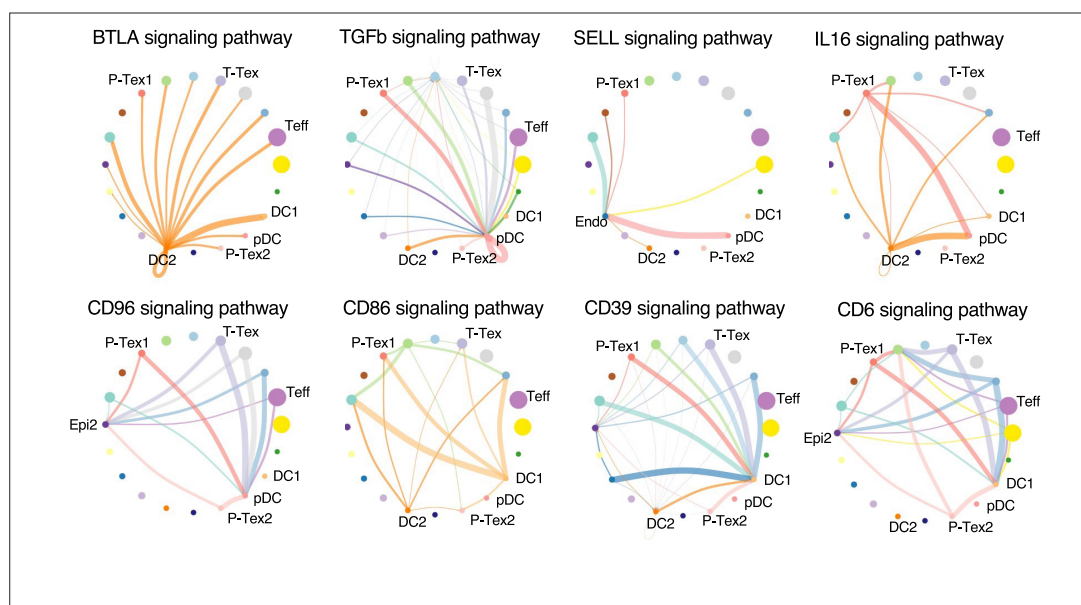


Figure 6—figure supplement 1. The supplementary cell–cell interactions of head and neck squamous cell carcinoma (HNSCC) tumor microenvironment (TME) for **Figure 6b**.



Figure 6—figure supplement 2. The correlation of Tex, P-Tex, and activation scores with APC scores for each cluster in spatial transcriptomics.

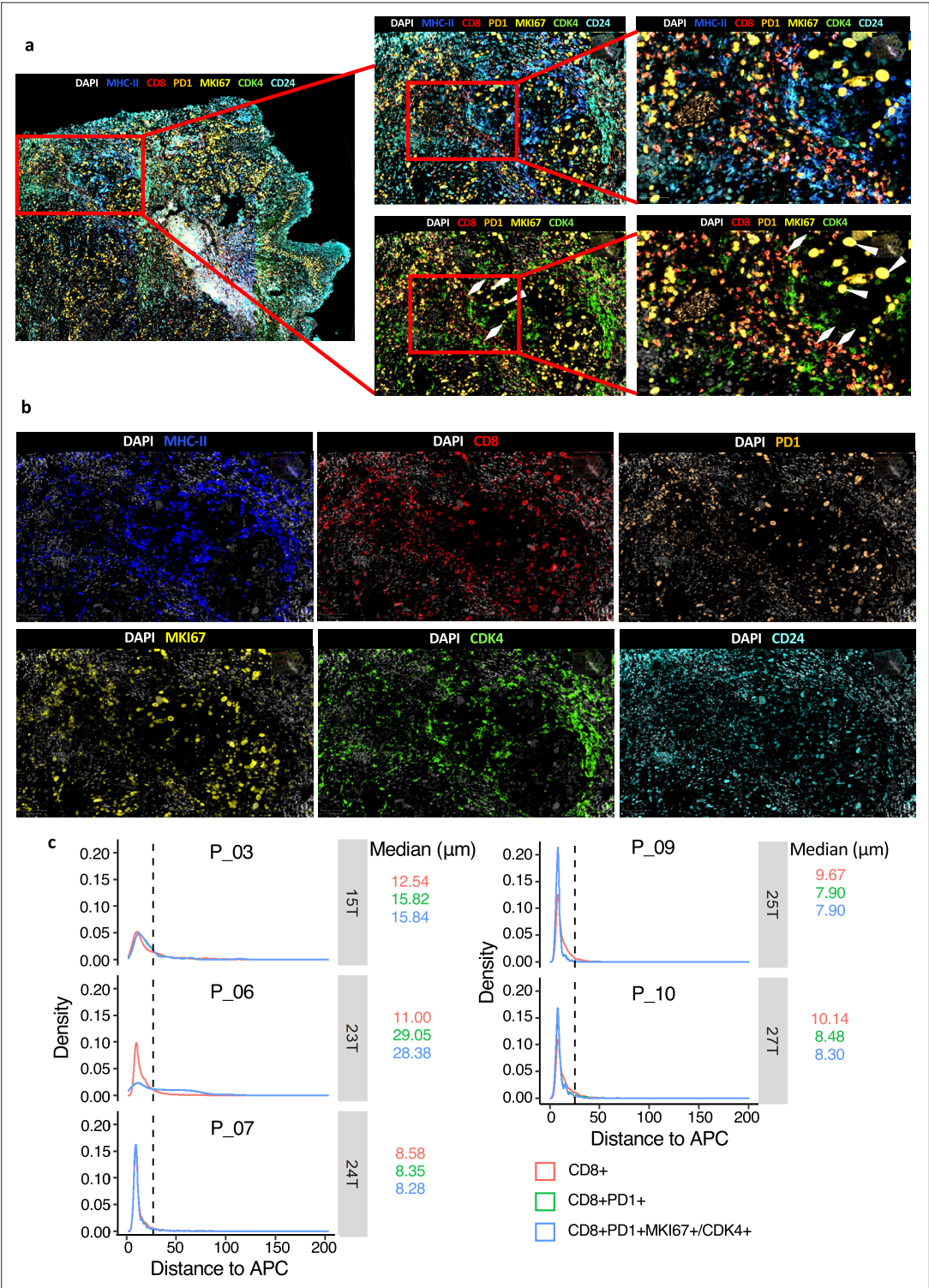


Figure 7. The spatial characteristics of APC, pro-Tex cells, and Tex cells in the head and neck squamous cell carcinoma (HNSCC) tumor microenvironment (TME). **(a–b)** Representative example of HNSCC tumor stained by multiplex IHC, with white triangles and rhombus showing the Texs and P-Tex aggregates in the APC area, respectively. **(c)** Measured distances to APC (MHCII⁺) cells from CD8⁺ T cells, CD8⁺ PD1⁺ T cells (Tex cells) or CD8⁺ PD1⁺ MKI67⁺/CDK4⁺ T cells (P-Tex cells) in five representative samples. The dashed lines represent the cutoff distance of 25 μm, which indicate that 90% of CD8⁺ T, Tex, or P-Tex cells are enriched within a distance of 25 μm from APCs.